IOP Publishing | Institute of Physics and Engineering in Medicine Physics in Medicine & Biology

Phys. Med. Biol. **61** (2016) 8825–8838 doi:10.1088/1361-6560/61/24/8825

Effect of microscopic modeling of skin in electrical and thermal analysis of transcranial direct current stimulation

Jose Gomez-Tames[1], Yukiya Sugiyama[1], Ilkka Laakso[2], Satoshi Tanaka[3], Soichiro Koyama[4], Norihiro Sadato[5,6] and Akimasa Hirata[1]

[1] Department of Computer Science and Engineering, Nagoya Institute of Technology, Nagoya, Japan
[2] Aalto University, Espoo, Finland
[3] Hamamatsu University School of Medicine, Hamamatsu, Japan
[4] Faculty of Rehabilitation, School of Health Sciences, Fujita Health University, Toyoake, Aichi, Japan
[5] National Institute for Physiological Sciences, Okazaki, Japan
[6] Department of Physiological Sciences, SOKENDAI (The Graduate University for Advanced Studies), Kanagawa, Japan

E-mail: ahirata@nitech.ac.jp

Received 15 July 2016, revised 29 August 2016
Accepted for publication 29 September 2016
Published 29 November 2016

Abstract

Transcranial direct current stimulation (tDCS) is a neuromodulation scheme where a small current is delivered to the brain via two electrodes attached to the scalp. The electrode design is an important topic, not only as regards efficacy, but also from a safety perspective, as tDCS may be related to skin lesions that are sometimes observed after stimulation. Previous computational models of tDCS have omitted the effects of microscopic structures in the skin, and the different soak conditions of the electrodes, and model validation has been limited. In this study, multiphysics and multiscale analysis are proposed to demonstrate the importance of microscopic modeling of the skin, in order to clarify the effects of the internal electric field, and to examine temperature elevation around the electrodes. This novel microscopic model of the skin layer took into consideration the effect of saline/water penetration in hair follicles and sweat ducts on the field distribution around the electrodes. The temperature elevation in the skin was then computed by solving the bioheat equation. Also, a multiscale model was introduced to account for macroscopic and microscopic tissues of the head and skin, which was validated by measurement of the head resistance during tDCS. As a result, the electric field in the microscopic model of the skin was less localized when the follicles/

ducts were filled with saline instead of hair or tap water. Temperature elevation was also lessened with saline, in comparison with other substances. Saline, which may penetrate the hair follicles and sweat ducts, suppressed the field concentration around the electrodes. For conventional magnitudes of current injection, and a head resistance of less than 10 kΩ, the temperature elevation in the skin when using saline–soaked electrodes was low, less than 0.1 °C, and unlikely to cause adverse thermal effects.

Keywords: skin modeling, brain stimulation, multi-scale modeling, direct current, electrode design

(Some figures may appear in colour only in the online journal)

1. Introduction

Over the last decade, brain stimulation has attracted considerable attention among neuroscientists (e.g. Nitsche *et al* 2008, Rossi *et al* 2009). Among other procedures, transcranial direct current stimulation (tDCS) is often applied in the course of motor and cognitive research (Tanaka and Watanabe 2009, Tanaka *et al* 2011, Elsner *et al* 2013, 2015). tDCS is a neuromodulation scheme, whereby a small current (a few milliamperes) is delivered to the brain via two electrodes attached to the scalp. Many clinical studies report its potential efficacy in improving motor function (Nitsche and Paulus 2000, Webster *et al* 2006, Roy *et al* 2014).

Electrode design is an important topic in tDCS, for not only in terms of efficacy but also of safety, evaluated by the current density distribution under the electrode (Nathan *et al* 1993, Bikson *et al* 2009, Minhas *et al* 2010). The volume conductor model, in which human tissues are expressed in terms of measured conductivity, is often used to investigate the internal electric field (Datta *et al* 2009a, Parazzini *et al* 2011, Brunoni *et al* 2012, Noetscher *et al* 2014, Wagner *et al* 2014, Laakso *et al* 2015, Saturnino *et al* 2015). Most studies have evaluated the internal electric field in the brain in order to discuss optimal electrode locations and design. Saturnino *et al* (2015) suggest that a low saline content (low conductivity) electrode would be beneficial, in order to generate a homogeneous field around the electrode.

The adverse effects of tDCS have been reported since the 2000s, and mild pain and transient redness in the skin have been documented (Bikson *et al* 2009, Loo *et al* 2011, Brunoni *et al* 2012). It was reported that, during treatments of five days per week over a two- or three-week period, lesions appeared after a few days of treatment, and continued to appear until the end of the treatment (Palm *et al* 2008, Frank *et al* 2010). The lesion size ranged from a few millimeters to 20 mm and was approximately proportional to skin resistance. In these studies, the electrodes were soaked in tap water, instead of a saline solution, to suppress itching, and an electroencephalogram was recorded immediately after the treatment. Mild redness in the hair follicles of the scalp was reported in Kasahara *et al* (2011) for an injection current of 1 mA. Further extensive data is summarized in (Poreisz *et al* 2007, Kuo *et al* 2014). A computational approach has revealed some possible causes of the adverse effect of current density distribution. The internal electric field in the skin was shown to be strong along the edges of the electrode (Miranda *et al* 2006, Minhas *et al* 2011). Moreover, the internal electric field in the skin of an anatomical head model was shown to be large for a typical electrode configuration, but insufficient to induce temperature elevation causing a burning sensation (Datta *et al* 2009b). In these studies, the effect of soaking the electrodes in water was not considered, and in general, the selection of electrodes and contact medium (Woods *et al* 2015) is inconsistent and not standardized. Also, the validation of the volume conductor model for tDCS is limited;

only one study compared the computed electrical potential with measurements (Bikson *et al* 2012); the resistance between the electrodes including the head is used as a metric when discussing side effects.

This study investigates for the first time a microscopic computational model of the skin, including stratum corneum, epidermis and dermis tissues with hair follicles and sweat ducts. Some microscopic discussion on skin modeling can be found in Huclova *et al* (2011) and Schmid *et al* (2013) for high and low frequencies, respectively. The effect on the internal electric field, and temperature elevation, are computed around the electrodes of saline/water penetration in hair follicles and sweat ducts during tDCS. In addition, multiscale simulations of the head were compared with experimental measurements in human participants, in order to validate the proposed microscopic skin model by reproducing tDCS conditions in the experiment. The side effects of tDCS, based on computation of the internal field and resultant temperature elevation, are discussed below, as is the importance of microscopic modeling of the skin.

2. Model and methods

2.1. Participants

The participants were seven male volunteers 28.9 (mean) $\pm$ 1.5 (standard deviation) years in age. The study was approved by the ethics committee of the National Institute for Physiological Sciences. None of the participants reported a history of neurological/psychiatric disorders or any other contraindication to tDCS.

2.2. tDCS

Current was applied using a DC-Stimulator (Eldith), which ceased instantaneously when resistance exceeded 13 kΩ, in order to avoid possible adverse effects. Because the resistance of the human head is largely affected by the skin condition, the skin was first wiped with gauze soaked in alcohol before the electrodes were attached. Rubber electrodes (1 mm thick) covered by a sponge (3 mm thick), which were soaked in normal saline, were attached above the ears, as shown in figure 1(a). This configuration was employed to hold both electrodes in place with a single belt around the head, simplifying the experiment and reducing human errors. The cerebral structure under the electrodes was the secondary somatosensory cortex (S2), which is important for somatosensory and pain perception. A previous study showed that tDCS over S2 yields an improvement in tactile discrimination performance (Fujimoto *et al* 2016). Thus, this configuration of electrodes might be useful for the treatment of patients with sensory deficits. This potential clinical application made us decide to apply tDCS just above the ears in the present study.

During stimulation, the current amplitude was increased linearly to 2 mA in the first 15 s, and kept constant for 600 s. After stimulation, the current was decreased gradually for 15 s. During stimulation, current, voltage, and resistance were recorded every 0.5 s. The resolution of the recorded resistance was within 0.1 kΩ. The same procedure was applied to measure the resistance between rubber electrodes connected directly, without a sponge.

2.3. Equivalent circuit model of tDCS System

A computational analysis was conducted for a multiscale model consisting of (i) the head without the skin layer and (ii) detailed layers of skin.

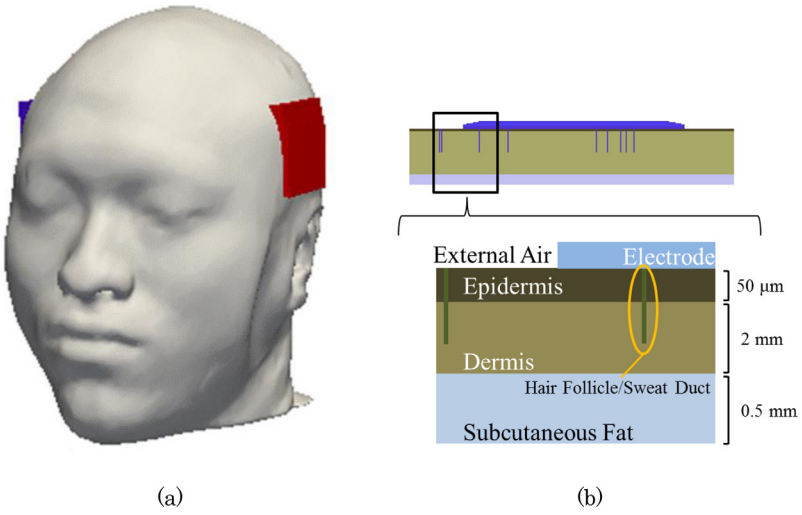

Figure 1. (a) Human head model with two electrodes attached (resolution of 500 μm) and (b) detailed skin layer model (resolution of 50 μm). The bottom of the skin model was truncated by an infinite metallic electrode.

The resistance of the human head is used as a metric for safety. It was considered as a series circuit comprising the skin and the remaining head resistances. This assumption is valid because of the linearity of Maxwell's equations and the high resistance of the skin, which prevented direct current flow from one electrode to the other; rather, the current flow was almost perpendicular to the head surface (e.g. Miranda *et al* 2006). The initial measured resistance of the two electrodes (rubber and sponge) in direct contact was in the range 1.5 kΩ–1.8 kΩ, and varied within 0.1 kΩ during the 600 s, suggesting that we can treat the electrodes with a sponge as a lumped element for an injection current of 2 mA. The equivalent circuit model for the system under consideration can be represented as shown in figure 2.

Skin resistance has nonlinear characteristics. However, for a current injection up to 100 μA cm^{-2}, resistance is almost constant (Yamamoto and Yamamoto 1981). Also, skin resistance may depend on time owing to osmotic dehydration caused by the saline solution in the sponge (Egawa *et al* 2007, Egawa and Kajikawa 2009). This will be discussed further in section 4.

2.4. Numerical head and skin models

A macroscopic analysis was conducted using anatomically-based human head models with a resolution of 0.5 mm. At this resolution, the skin cannot be appropriately evaluated. Therefore, a separate simplified skin model with a resolution of 50 μm was considered in a microscopic analysis. A discussion of microscopic skin modeling can be found in (Huclova *et al* 2011, Schmid *et al* 2013); electromagnetic modeling of the skin is also listed as a topic to be resolved by IEEE International Committee on Electromagnetic Safety (Reilly and Hirata 2016). Twenty-four head models with a resolution of 0.5 mm, comprising 10 anatomical tissues, were constructed from magnetic resonance images as described in Laakso *et al* (2015). The reason for this is in order to examine the variability of head resistance, especially for internal morphology. Electrodes (50 mm $\times$ 50 mm) were attached to the head models, as shown in figure 1(a). The skin was not modeled in the macroscopic analysis. As discussed in Laakso *et al* (2015), scalp thickness did not have a statistically significant effect on the electric field in the brain.

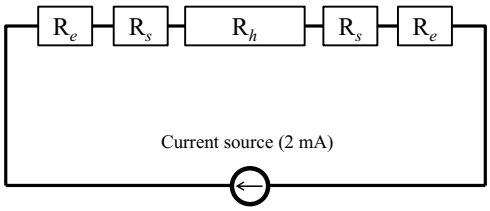

Figure 2. Equivalent circuit model of the tDCS system. R_e, R_s, and R_h are the resistance of the rubber electrode with a sponge, the skin layer (2 mm thickness), and the head model excluding the skin, respectively.

The simplified skin model used in the microscopic analysis is shown in figure 1(b), in which skin pores, comprising hair follicles and sweat ducts, were modeled approximately. Its impedance is an independent element of the circuit model of the tDCS system in figure 2. The thicknesses of the epidermis, dermis, and subcutaneous fat were 50 μm or 100 μm, 2 mm, and 0.5 mm, respectively. The horizontal dimensions were 45 mm $\times$ 45 mm. The diameters of the hair follicles and sweat ducts were 50 μm (matching the model resolution) with spatial densities of 1–2 per mm^2 and 7–9 per mm^2, respectively. Three models were considered: hair follicles and sweat ducts filled with (a) saline and (b) tap water, as well as (c) hair follicles filled with hair, where sweat ducts are assumed as air. The locations of hair follicles and sweat ducts were determined randomly.

In the analysis of skin resistance, the bottom of the model was truncated by a perfect conductor to compute the resistance of the skin layer. The electrode size was assumed to be 10 mm $\times$ 10 mm, which is smaller than that used in the measurement, owing to the limitations of computational memory. However, resistance was extrapolated for an electrode size of 50 mm $\times$ 50 mm, using the inverse relationship between resistance and area.

For the analysis of thermal computation, a fat layer of 10 mm of thickness was added in order to compute temperature elevation appropriately.

2.5. Volume conductor modeling

Electric field dosimetry was conducted separately for the macroscopic and microscopic models. In a regime where displacement current can be disregarded, the volume conductor model is often used to investigate the internal electric field in biological tissue, not only in the case of tDCS, but also for transcranial magnetic stimulation (Laakso and Hirata 2012b, Cvetkovic *et al* 2015, Lu and Ueno 2015). The scalar potential finite difference method (Dawson and Stuchly 1998) is used to solve scalar potential equation:

$$\nabla(\sigma\,\nabla(\phi)) = 0 \tag{1}$$

where φ and σ denote scalar potential and tissue conductivity, respectively.

By defining scalar potentials (unknowns) at each node of a cubic voxel (the minimum component of the model was 9.1 $\times$ 10^6 voxels in this study), a branch current flowing from one node to a neighboring node along the side of the voxels was derived, which included a scalar potential due to the applied electric charge and impedance between the nodes. By applying Kirchhoff's current law at all nodes, simultaneous equations were then set. The potential was solved iteratively, using the successive-over-relaxation method and multigrid method (Laakso and Hirata 2012b). Possible numerical uncertainties were minimized by smoothing the conductivity contrast between adjacent tissues, including the high contrast between follicles or sweat ducts, and the surrounding medium (Laakso and Hirata 2012c).

The electric field along the edge of the voxel was obtained by dividing the difference in potential between the nodes of the voxel by the distance across the nodes, and adding the vector potential. The number of multigrid levels was six, and the iteration continued until the relative residual was less than 10^{-6} (Laakso and Hirata 2012a); for this residual, the error relative to the maximum internal electric field was less than 0.5%.

The specific energy absorption rate was calculated as:

$$\mathrm{SAR} = \frac{\sigma}{\rho}|E|^2 \tag{2}$$

where ρ denotes the mass density of the tissue.

Head tissue conductivities are shown in table 1(a) (supplementary material in Laakso *et al* (2015)). The epidermis (stratum corneum) and dermis in table 1(b) were taken from Yamamoto and Yamamoto (1976). The average epidermal stratum corneum was interpolated to direct current (6.6×10^{-6} S m^{-1}). The conductivity of the dermis (innermost keratin layer) was 0.003 S m^{-1}. The conductivities of tap water (in Japan) and hair were taken from HoribaLtd (1996) and van Orden (1998), respectively. The conductivity of tap water may vary by a factor of 2 (~0.03 S m^{-1}) (Torrents *et al* 2001). The highest uncertainty was attributed to the value for the dermis, which has not been reported until now (except simply as skin). Thus, assuming that the conductivity of the dermis was somewhere between that of the epidermis and the subcutaneous fat, an uncertainty analysis was assumed for values from 0.003 S m^{-1} to 0.03 S m^{-1} (approximately the average conductivity of the epidermis and fat). The conductivity of the dermis in Yamamoto and Yamamoto (1976) was similar to the skin conductivity presented in Gabriel *et al* (1996).

For our computation, a current source was applied between the two electrodes. Resistance was then calculated as the electric potential difference between the two electrodes, divided by the applied current, which is one of the main metrics used for validating the computational results hereinafter. The resistance of the human head is often used as a metric for side-effects.

2.6. Thermal modeling

Thermal modeling for tDCS safety is limited (Datta *et al* 2009b). We conducted thermal dosimetry only for the skin-layer model (microscopic model). The temperature in the human model was calculated by numerically solving the following bioheat equation (Pennes 1948), which considers various heat exchange mechanisms, including the heat conduction, blood perfusion, and resistive heating:

$$\begin{aligned} C(\boldsymbol{r})\rho(\boldsymbol{r})\frac{\partial T(\boldsymbol{r},t)}{\partial t} &= \nabla\cdot\left(K(\boldsymbol{r})\nabla T(\boldsymbol{r},t)\right) + \rho(\boldsymbol{r})\mathrm{SAR}(\boldsymbol{r}) \\ &\quad + Q(\boldsymbol{r},t) - B(\boldsymbol{r},t)\left(T(\boldsymbol{r},t) - T_{\mathrm{B}}(\boldsymbol{r},t)\right) \end{aligned} \tag{3}$$

where T, K, and C are the temperature, thermal conductivity, and specific heat of the tissue, respectively; T_{B} is blood temperature (37 °C), Q is the metabolic heat generation, B is the parameter associated with the blood perfusion, and $\boldsymbol{r}$ is the position vector.

Equation (3) was subjected to the following boundary condition:

$$-K(\boldsymbol{r})\frac{\partial T(\boldsymbol{r},t)}{\partial n} = H\cdot\left(T_{\mathrm{s}}(\boldsymbol{r},t) - T_{\mathrm{e}}(t)\right) \tag{4}$$

where H, T_{s}, and T_{e} denote the heat-transfer coefficient, surface temperature of the tissue, and temperature of the air, respectively. The boundaries of the side and the bottom of the skin layer model (figure 1(b)), where the temperature was assumed to be constant, were truncated by

Table 1. Conductivities of human head tissues. The same values for fat conductivities were used for (a) macroscopic head and (b) microscopic skin-layer models.

(a)	
Tissue	σ (S m^{-1})
Blood	0.7
Bone cancellous	0.06
Bone cortical	0.013
Gray matter	0.10
White matter	0.10
Cerebrospinal fluid	1.8
Eye (vitreous)	1.5
Muscle	0.16
Fat	0.08
(b)	
Epidermis	6.6×10^{-6}
Dermis	3.0×10^{-3}
Fat	8.0×10^{-2}
Saline	1.4
Tap Water	1.5×10^{-2}
Hair	1.65×10^{-5}

the approximate boundary condition. The size of the selected computational region was large enough so as not to affect the computed temperature distribution; if the computational region was enlarged by 50%, the resultant temperature elevation around the computational region was affected by a few percent or less.

The bioheat equation subjected to the boundary condition was solved to investigate the resulting temperature elevation in the thermal steady state. Thus, the left-hand side term of (3) was assumed to be zero. The equation was discretized using a finite- difference method, and solved by applying the geometric multigrid method (Laakso 2009).

The thermal parameters and mass densities used in the present study were mainly taken from Janssen *et al* (2005), as shown in table 2. The thermal parameters of the soaked electrodes were assumed to be the same as those of saline. When the electrodes were not soaked, the parameters were assumed to be those of hair, owing to lack of data. The heat-transfer coefficient between the model surface and air was set as 5 W m^{-2} °C^{-1}, which is the typical value at room temperature, i.e. 23 °C (Fiala *et al* 1999). The temperature below the fat layer is assumed as 37 °C. The initial condition was then derived assuming no SAR or power disposition exists.

An uncertainty factor in the resultant temperature elevation would be the blood flow in the skin, which may be affected by the pressure when attaching the electrodes. However, due to the lack of the data, this uncertainty is not discussed in this study.

3. Results

3.1. Measured resistance of head and electrodes

The time evolution of the resistance measured during the tDCS treatment is shown in figure 3. The resistance of the two electrodes with wet sponge in direct contact was between 1.5 kΩ and 1.8 kΩ ($2R_e$), where the variability may have been caused by the pressure contact. When

Table 2. Thermal parameters of skin layer model.

Tissue	Thermal conductivity K (W m^{-1} · K^{-1})	Specific heat C (J kg^{-1} · K^{-1})	Blood flow B (W (m^{-3} · K^{-1}))	Metabolic rate Q (W m^{-3})
Epidermis	0.42	3600	3687	1620
Dermis	0.42	3600	3687	1620
Fat	0.25	3000	1626	3000
Tap water	0.56	4220	0	0
Saline	0.62	4000	0	0
Hair	0.26	1000	0	0

the two rubber electrodes were connected directly without a sponge or soakage in water/saline solution, the maximum resistance was 0.1–0.2 kΩ. The higher impedance in the presence of the sponge was mostly originated from the rubber-sponge interface. This was confirmed by measuring the electrode resistance of the two electrodes with wet sponge in direct contact at 10 Hz, and 240 Hz. The resistance was reduced to 0.1–0.2 kΩ (similar to the two rubber electrodes).

The measured resistance ($R_h + 2R_s + 2R_e$) had a large variability in the range of 2.8–5.7 kΩ at the initial state ($t = 0$), corresponding to a head resistance ($R_h + 2R_s$; excluding two electrodes) of 1.0–4.2 kΩ. The head resistance then gradually decreased during the 10 min of stimulation, corresponding to a head resistance of 0.4–2.4 kΩ. This decrease was 42–61% with respect to the initial resistance.

3.2. Computed resistance for head and skin models

The resistance of the 24 macroscopic head models without the skin (R_h) was calculated as 213 ± 11 Ω using a similar computational setup as described in Laakso *et al* (2015). To incorporate the resistance of the skin, the multilayer skin model (figure 1(b)) was considered. The computed skin resistances for hair follicles/sweat ducts filled with saline, tap water, and hair are presented in table 3. As shown in the table, the resistance of the skin was affected by the contents of follicles/ducts, as well as the thickness of the epidermis. The resistance was relatively low when the follicles/ducts were filled with saline. This difference was caused by differences in conductivity between saline, tap water, and hair. The skin resistance was dominant in the total head resistance, which is consistent with Yamamoto and Yamamoto (1976).

The computed resistance of the head without the skin (R_h) was 213 Ω, as previously mentioned. Thus, the computed resistance of the human head with the skin (R_s, table 3) was in the range of 729–1443 Ω for variable densities of hair follicles and sweat ducts. The computed resistance of the human head with the skin pores filled with saline solution ($R_h + 2R_s$) was estimated as 729–1041 Ω. This falls within the range of values measured at the end of the experiment: 0.4–2.4 kΩ (see section 3.1). The resistance of the head with the skin pores filled with hair or tap water was calculated to be 1157–1443 Ω, which is within the range of values measured at the start of the experiment: 1.0–4.2 kΩ.

3.3. Computed electric field and temperature elevation distributions in the skin

The electric field on the model surface is illustrated in figure 4 for the multilayer skin model with follicles/ducts filled with saline solution, tap water, and hair. As shown in figure 4(A-a), the electric field on the model with follicles/ducts filled with saline solution (light blue grains) was rather smooth in the epidermis, and the high electric field around the electrode edges was

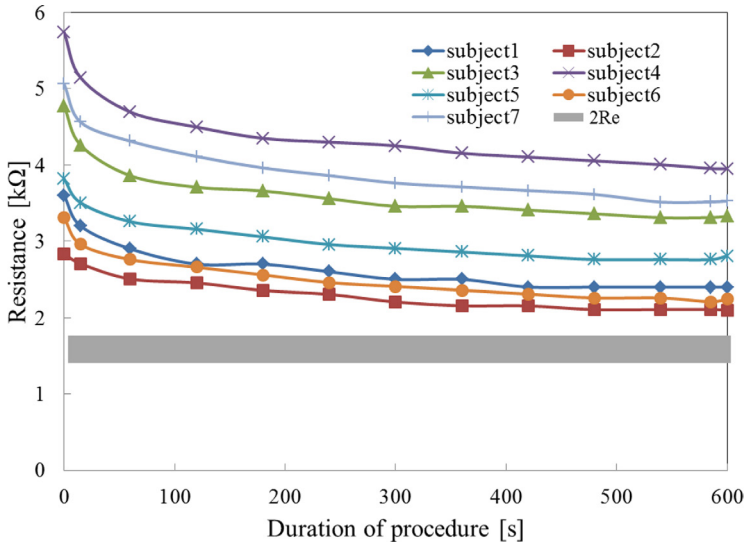

Figure 3. Resistance variation seen from the electrodes during tDCS treatment for 7 participants ($R_h + 2R_s + 2R_e$). Variability of resistance between two electrodes ($2R_e$) in direct contact is also presented to derive human head resistance ($R_h + 2R_s$).

Table 3. Resistance (Ω) of skin layer (R_s) with hair follicles and duct densities of (i) lowest, (ii) averaged, and (iii) highest densities adjusted for $5 \times 5\,cm^2$ of electrode size. The epidermis thickness was chosen as 50 μm and 100 μm. The calculated head resistance can be calculated by $R_h + 2R_s$, where $R_h = 213\ \Omega$.

	50 μm			100 μm		
Thickness density	Low	Mean	High	Low	Mean	High
Saline	371	349	326	414	336	258
Tap water	485	477	472	566	553	540
Hair	490	491	492	611	613	615

not obvious, because of the high conductivity of saline compared with tap water and hair. On the other hand, when the follicles/ducts were filled with hair only (figure 4(A-c)), the electric field around the edges was most evident, corresponding with previous findings (Miranda *et al* 2006). For deeper epidermis tissue (figure 4(B)), a higher electric field was observed at the end tip of the follicles and sweat ducts (light blue) for saline solution, due to a higher current density in the highly conductive follicles. In the subcutaneous fat tissue, a close electric field distribution can be found for the three configurations; however, saline produced a less symmetric field pattern.

The distribution of the temperature elevation calculated by specific absorption rate as a heat source is shown in figure 5. Figure 5(a) shows that the temperature elevation was smallest when the follicles/ducts were filled with saline solution, and as shown in figures 5(b) and (c), the temperature elevation was almost identical when the follicles/ducts were filled with hair and tap water. Furthermore, the distribution of the temperature elevation differed from that of the electric field; the temperature was elevated at the centre rather than at the edges of the electrode. The temperature elevation around the electrode was marginally affected, even for an electrode with a larger horizontal dimension (see section 2.3).

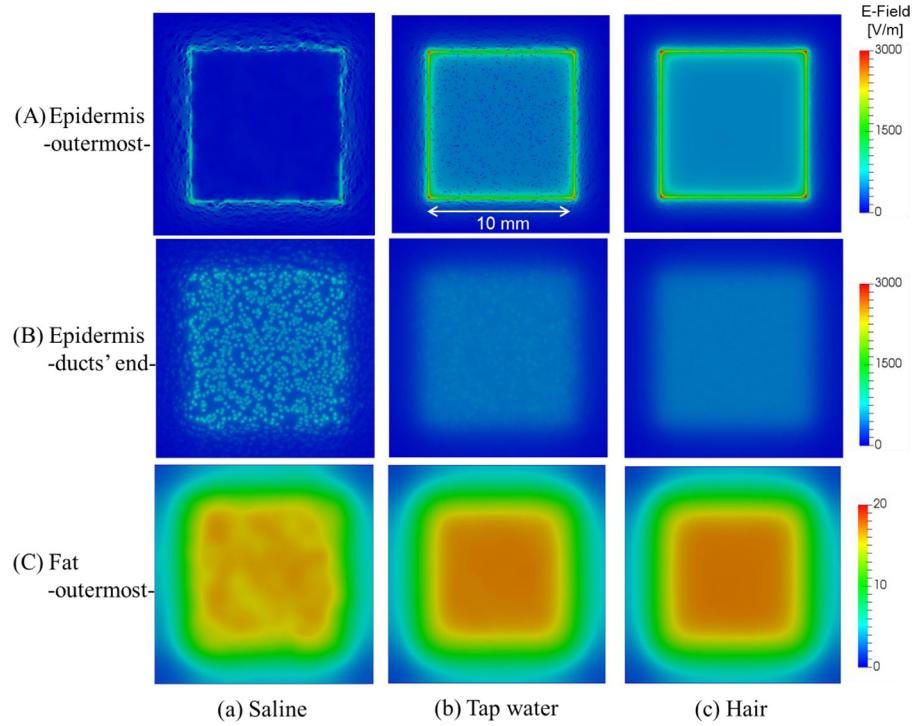

Figure 4. *In situ* electric field in three locations: (A) outermost layer of epidermis (50 μm from electrode-skin interface), (B) end tip of follicles and sweat ducts (1 mm), and (C) outermost layer of subcutaneous fat tissue (2 mm) for (a) saline, (b) tap water, and (c) hair. The thickness of the epidermis is 50 μm and the maximum density of hair follicles and duct densities are used.

4. Discussion

One of the main elements of this study is that the resistance of the head was estimated using the multiscale head model (macroscopic model of the head and microscopic model of the skin), and validated with experimental measurements. Also, computational analysis of electric and thermal effects of tDCs in the skin was conducted.

The resistances of the human head without the skin were calculated and demonstrated to be $213 \pm 11\ \Omega$ for 24 head models developed from MR images. As the head-model anatomy may depend on the classification algorithm, we also computed the head resistance using Japanese adult male model without the skin (Nagaoka *et al* 2004). A resistance of 210 Ω was obtained, which is within the standard variation of the 24 models. In contrast, skin conductivity is highly variable, dependent on the wetness and microscopic structure of the skin, and several measured values have been reported by different researchers (Yamamoto and Yamamoto 1977). Thus, a model of the microscopic structure of the skin, including follicles and sweat ducts, can obtain information on skin impedance variability and effects in the distribution of the electric field under the electrode in far greater detail, as shown in figure 4.

We computed the skin resistance using a resolution of 50 μm. Even when a model with a resolution of 25 μm is used, no significant variation of the electric field distribution was observed. The mean error between different resolutions was 12.2% of the maximum electric field in each plane below the electrodes for the case of mean density and saline solution. Its effect on the skin impedance variation was 4.5%.

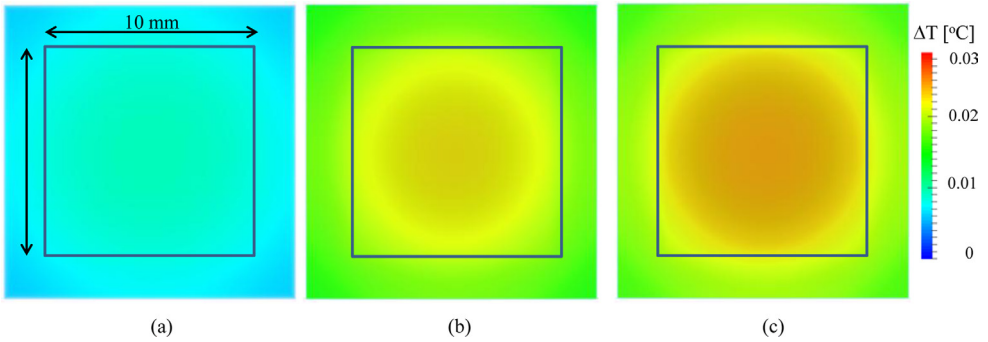

Figure 5. Temperature elevation on the epidermis for (a) saline, (b) tap water, and (c) hair. The dimensions corresponding to the electrode (10 mm × 10 mm) are also indicated. The thickness of the epidermis is 50 μm and the mean values of hair follicles and duct densities are used.

We confirmed that the inter- and intra-subject variability in the resistance is attributable to skin condition, which is the main source of the head resistance, as shown in table 3. When we empirically changed the conductivity of the dermis by one order of magnitude (see section 2.3), the skin resistance changed by 15% or less, which did not affect the agreement between experimental and computed resistance of the human head. In addition, the boundaries among the stratum corneum, epidermis, and dermis are not easily expressed, because they were rippled depending on the location. These factors may have caused the remaining variability in our computation.

The measured and computed resistances of the human head (excluding the electrodes) matched with saline and hair and saline conditions at the start and end of the experiment, respectively, where the resistance was 0.7–1.8 kΩ smaller at the end of the treatment. It is speculated that the variations in initial resistance were caused by factors such as the resistance of the hair, the condition of the skin pores (e.g. pore-clogging debris), the contact condition of the electrodes with the skin, and the osmotic dehydration caused by the saline solution in the sponge (Egawa *et al* 2007, Egawa and Kajikawa 2009). Also, the water content of the stratum corneum increases with the water-application time, which may increase the conductivity (Egawa and Kajikawa 2009). The reduction of the head resistance in the experiment was roughly estimated as the difference between the resistance of the skin filled with hair and saline: 152–714 Ω, derived from table 3. This reduction is comparable to, or lower than, the minimum reduction of the resistance (0.7 kΩ) observed in the experiment. The good agreement between the measured and computed resistances, assuming saline-filled follicles, suggests the effectiveness of multiscale modeling, and the accuracy of our hypothesis that the reduction of the resistance was caused by osmotic dehydration.

When the electrode was soaked in saline, the field concentration around the edge of the electrode disappeared. This change is attributed to the high conductivity of saline compared with tap water and hair (figure 4). Thus, the field concentration at the electrode edge reported in Miranda *et al* (2006) may not be evident for electrodes soaked in a saline solution. This finding differs from previous conclusions, derived from macroscopic modeling only: less saline produces a more uniform field distribution (Saturnino *et al* 2015).

The temperature elevation was at most 0.1 °C or less, due to power absorption (figure 5). This marginal temperature elevation is difficult to confirm, but using thermography the temperature distributions before and after the treatment were not almost identical, although not shown here. This temperature elevation was sufficiently small compared with 1–2 °C (ICNIRP 1998), a reference value for the temperature elevation in human-safety guidelines

(not medical equipment). It should be noted that skin damage has been reported at 43 °C, which corresponds to a temperature elevation of 7–8 °C (Hardy *et al* 1951). In addition, unlike the power-absorption distribution, the temperature-elevation distribution was more spread out because of the diffusion of heat (Hirata *et al* 2006). In our computation, the skin surface was assumed to be uniform. However, because of factors such as the existence of hair and the contact area of the electrodes, the internal electric field may not have been uniform, resulting in a concentration of the power absorption and temperature elevation.

For the resistance values of 30–55 kΩ reported in Palm *et al* (2008), the temperature elevation at the injection current of 2 mA was estimated to be 1.2–2.2 °C, which is higher but comparable to the aforementioned threshold for thermal damage. The limitation of thermal modeling is that the non-uniform power absorption was not considered in the electrodes, and the rubber was not modeled in the electrodes. Also, no skin lesions were observed when the electrode sponges were regularly replaced (Frank *et al* 2010). Another possible cause of side-effects is the chemical reaction between the electrodes and saline solution, discussed extensively in Minhas *et al* (2010). Also, a double layer effect between the electrode-skin interface can be considered for short pulse stimulation. However, this is outside the scope of this study, which only considered the physical aspects over long stimulation periods. Finally, this study demonstrates the importance of considering multiscale analysis by considering microscopic structures in the skin for field distributions near the electrode. The next step is to extend this approach to investigate its effects on brain field distribution for tDCS or other neurostimulation techniques.

5. Conclusions

A multiscale skin model was employed to calculate the resistance of the head for the first time. The electric field in the skin differed according to the medium of the hair follicles/sweat ducts. When the follicles/ducts were filled with a saline solution, the localization of the electric field around the edges of the electrode was suppressed because the follicles/ducts behaved as current paths. Our computational results suggest that, although the mechanism of the adverse effects of the tDCS treatment is unclear from a physics viewpoint, the electrodes soaked in saline solution suppressed these effects; this data could not have been obtained without a finer skin model. Moreover, it was confirmed that temperature elevation in the skin due to saline-soaked electrodes was not high enough to induce thermal damage for a typical head resistance. The recommendation of a low saline (low conductivity) electrode for the generation of a homogeneous field around the electrode, as concluded by Saturnino *et al* (2015), may not be appropriate, based on this microscopic modeling. This computational modeling may be useful when designing and evaluating tDCS electrodes.

References

Bikson M, Datta A and Elwassif M 2009 Establishing safety limits for transcranial direct current stimulation *Clin. Neurophysiol.* **120** 1033

Bikson M, Rahman A and Datta A 2012 Computational models of transcranial direct current stimulation *Clin. EEG Neurosci.* **43** 176–83

Brunoni A R *et al* 2012 Clinical research with transcranial direct current stimulation (tDCS): challenges and future directions *Brain Stimul.* **5** 175–95

Cvetkovic M, Poljak D and Haueisen J 2015 Analysis of transcranial magnetic stimulation based on the surface integral equation formulation *IEEE Trans. Biomed. Eng.* **62** 1535–45

Datta A, Bansal V, Diaz J, Patel J, Reato D and Bikson M 2009a Gyri-precise head model of transcranial direct current stimulation: improved spatial focality using a ring electrode versus conventional rectangular pad *Brain Stimul.* **2** 201–7

Datta A, Elwassif M and Bikson M 2009b Bio-heat transfer model of transcranial DC stimulation: comparison of conventional pad versus ring electrode *Proc. Annual Int. Conf. IEEE Eng. Med. and Biol. Soc.* (IEEE) pp 670–3

Dawson T W and Stuchly M A 1998 High-resolution organ dosimetry for human exposure to low-frequency magnetic fields *IEEE Trans. Mag.* **34** 708–18

Egawa M, Hirao T and Takahashi M 2007 *In vivo* estimation of stratum corneum thickness from water concentration profiles obtained with Raman spectroscopy *Acta. Derm. Venereol.* **87** 4–8

Egawa M and Kajikawa T 2009 Changes in the depth profile of water in the stratum corneum treated with water *Skin Res. Tech.* **15** 242–9

Elsner B, Kugler J, Pohl M and Mehrholz J 2013 Transcranial direct current stimulation (tDCS) for improving function and activities of daily living in patients after stroke *Cochrane Libr.* **11** 1–101

Elsner B, Kugler J, Pohl M and Mehrholz J 2015 Transcranial direct current stimulation (tDCS) for improving aphasia in patients with aphasia after stroke *Cochrane Libr.* **5** 1–61

Fiala D, Lomas K J and Stohrer M 1999 A computer model of human thermoregulation for a wide range of environmental conditions: the passive system *J. Appl. Physiol.* **87** 1957–72

Frank E, Wilfurth S, Landgrebe M, Eichhammer P, Hajak G and Langguth B 2010 Anodal skin lesions after treatment with transcranial direct current stimulation *Brain Stimul.* **3** 58–9

Fujimoto S, Kon N, Otaka Y, Yamaguchi T, Nakayama T, Kondo K, Ragert P and Tanaka S 2016 Transcranial direct current stimulation over the primary and secondary somatosensory cortices transiently improves tactile spatial discrimination in stroke patients *Front. Neurosci.* **10** 1–9

Gabriel S, Lau R W and Gabriel C 1996 The dielectric properties of biological tissues: III. Parametric models for the dielectric spectrum of tissues *Phys. Med. Biol.* **41** 2271–93

Hardy J D, Goodell H and Wolff H G 1951 The influence of skin temperature upon the pain threshold as evoked by thermal radiation *Science* **114** 149–50

Hirata A, Fujimoto M, Asano T, Wang J, Fujiwara O and Shiozawa T 2006 Correlation between maximum temperature increase and peak SAR with different average schemes and masses *IEEE Trans. Electromagn. Compat.* **48** 569–77

HoribaLtd 1996 What is electrical conductivity? www.horiba.com/jp/horiba-advanced-techno/hatwave/vol2/f_s_dic/ (Accessed: 20 August 2016)

Huclova S, Erni D and Fröhlich J 2011 Modelling and validation of dielectric properties of human skin in the MHz region focusing on skin layer morphology and material composition *J. Phys. D: Appl. Phys.* **45** 025301

ICNIRP 1998 Guidelines for limiting exposure to time-varying electric, magnetic, and electromagnetic fields (up to 300 GHz) *Health Phys.* **74** 494–521

Janssen F, Van Leeuwen G and Van Steenhoven A 2005 Modelling of temperature and perfusion during scalp cooling *Phys. Med. Biol.* **50** 4065

Kasahara K, Tanaka S, Watanabe K, Hanakawa T and Honda M 2011 Small skin lesion after treatment with repeated daily transcranial direct current stimulation (in Japanese) *Japan. J. Clin. Neurophys.* **39** 24–7

Kuo M-F, Paulus W and Nitsche M A 2014 Therapeutic effects of non-invasive brain stimulation with direct currents (tDCS) in neuropsychiatric diseases *Neuroimage* **85** 948–60

Laakso I 2009 Assessment of the computational uncertainty of temperature rise and SAR in the eyes and brain under far-field exposure from 1 to 10 GHz *Phys. Med. Biol.* **54** 3393

Laakso I and Hirata A 2012a Computational analysis of thresholds for magnetophosphenes *Phys. Med. Biol.* **57** 6147–65

Laakso I and Hirata A 2012b Fast multigrid-based computation of the induced electric field for transcranial magnetic stimulation *Phys. Med. Biol.* **57** 7753–65

Laakso I and Hirata A 2012c Reducing the staircasing error in computational dosimetry of low-frequency electromagnetic fields *Phys. Med. Biol.* **57** N25–34

Laakso I, Tanaka S, Koyama S, De Santis V and Hirata A 2015 Inter-subject variability in electric fields of motor cortical tDCS *Brain Stimul.* **8** 906–13

Loo C, Martin D, Alonzo A, Gandevia S, Mitchell P and Sachdev P 2011 Avoiding skin burns with transcranial direct current stimulation: preliminary considerations *Int. J. Neuropsychopharm.* **14** 425–6

Lu M and Ueno S 2015 Computational study toward deep transcranial magnetic stimulation using coaxial circular coils *IEEE Trans. Biomed. Eng.* **62** 2911–9

Minhas P, Bansal V, Patel J, Ho J S, Diaz J, Datta A and Bikson M 2010 Electrodes for high-definition transcutaneous DC stimulation for applications in drug delivery and electrotherapy, including tDCS *J. Neurosci. Meth.* **190** 188–97

Minhas P, Datta A and Bikson M 2011 Cutaneous perception during tDCS: role of electrode shape and sponge salinity *Clin. Neurophysiol.* **122** 637
Miranda P C, Lomarev M and Hallett M 2006 Modeling the current distribution during transcranial direct current stimulation *Clin. Neurophysiol.* **117** 1623–9
Nagaoka T, Watanabe S, Sakurai K, Kunieda E, Taki M and Yamanaka Y 2004 Development of realistic high-resolution whole-body voxel models of Japanese adult males and females of average height and weight, and application of models to radio-frequency electromagnetic-field dosimetry *Phys. Med. Biol.* **49** 1–15
Nathan S S, Sinha S R, Gordon B, Lesser R P and Thakor N V 1993 Determination of current density distributions generated by electrical stimulation of the human cerebral cortex *Electroencephalogr. Clin. Neurophysiol.* **86** 183–92
Nitsche M and Paulus W 2000 Excitability changes induced in the human motor cortex by weak transcranial direct current stimulation *J. Physiol.* **527** 633–9
Nitsche M A *et al* 2008 Transcranial direct current stimulation: state of the art *Brain Stimul.* **1** 206–23
Noetscher G M, Yanamadala J, Makarov S N and Pascual-Leone A 2014 Comparison of cephalic and extracephalic montages for transcranial direct current stimulation—a numerical study *IEEE Trans. Biomed. Eng.* **61** 2488–98
Palm U, Keeser D, Schiller C, Fintescu Z, Reisinger E, Padberg F and Nitsche M 2008 Skin lesions after treatment with transcranial direct current stimulation (tDCS) *Brain Stimul.* **1** 386–7
Parazzini M, Fiocchi S, Rossi E, Paglialonga A and Ravazzani P 2011 Transcranial direct current stimulation: estimation of the electric field and of the current density in an anatomical human head model *IEEE Trans. Biomed. Eng.* **58** 1773–80
Pennes H H 1948 Analysis of tissue and arterial blood temperatures in the resting human forearm *J. Appl. Physiol.* **1** 93–122
Poreisz C, Boros K, Antal A and Paulus W 2007 Safety aspects of transcranial direct current stimulation concerning healthy subjects and patients *Brain Res. Bull.* **72** 208–14
Reilly J P and Hirata A 2016 Low-frequency electrical dosimetry: research agenda of the IEEE International Committee on Electromagnetic Safety *Phys. Med. Biol.* **59** R138–49
Rossi S, Hallett M, Rossini P M, Pascual-Leone A and Group S o T C 2009 Safety, ethical considerations, and application guidelines for the use of transcranial magnetic stimulation in clinical practice and research *Clin. Neurophysiol.* **120** 2008–39
Roy A, Baxter B and Bin H 2014 High-definition transcranial direct current stimulation induces both acute and persistent changes in broadband cortical synchronization: a simultaneous tDCS EEG study *IEEE Trans. Biomed. Eng.* **61** 1967–78
Saturnino G B, Antunes A and Thielscher A 2015 On the importance of electrode parameters for shaping electric field patterns generated by tDCS *Neuroimage* **120** 25–35
Schmid G, Cecil S and Überbacher R 2013 The role of skin conductivity in a low frequency exposure assessment for peripheral nerve tissue according to the ICNIRP 2010 guidelines *Phys. Med. Biol.* **58** 4703–16
Tanaka S, Sandrini M and Cohen L G 2011 Modulation of motor learning and memory formation by non-invasive cortical stimulation of the primary motor cortex *Neuropsychol. Rehabil.* **21** 650–75
Tanaka S and Watanabe K 2009 Transcranial direct current stimulation—a new tool for human cognitive neuroscience *Brain Nerve* **61** 53–64
Torrents J, Mason T, Peled A, Shah S and Garboczi E 2001 Analysis of the impedance spectra of short conductive fiber-reinforced composites *J. Mater. Sci.* **36** 4003–12
van Orden M 1998 Hair conductivity tests www.rafischer.com/hairtest.htm (Accessed: 20 August 2016)
Wagner S, Rampersad S, Aydin Ü, Vorwerk J, Oostendorp T, Neuling T, Herrmann C, Stegeman D and Wolters C 2014 Investigation of tDCS volume conduction effects in a highly realistic head model *J. Neural Eng.* **11** 016002
Webster B R, Celnik P A and Cohen L G 2006 Noninvasive brain stimulation in stroke rehabilitation *NeuroRx* **3** 474–81
Woods A *et al* 2015 A technical guide to tDCS, and related non-invasive brain stimulation tools *Clin. Neurophysiol.* **127** 1031–48
Yamamoto T and Yamamoto Y 1976 Electrical properties of the epidermal stratum corneum *Med. Biol. Eng.* **14** 151–8
Yamamoto T and Yamamoto Y 1977 Analysis for the change of skin impedance *Med. Biol. Eng. Comput.* **15** 219–27
Yamamoto T and Yamamoto Y 1981 Non-linear electrical properties of skin in the low frequency range *Med. Biol. Eng. Comput.* **19** 302–10